# Reduction in Production pHEMT Process Variation Due to MBE Rotational Effects

W. Andrew Shelton and Clayton L. Workman

RF Micro Devices, Inc., 7628 Thorndike Road, Greensboro, NC 27409-9421
ashelton@rfmd.com, 336.678.5833

**Keywords: pHEMT, MBE, rotation, Vpo, sheet resistance**

**Abstract**

**Continuous azimuthal rotation is one method of minimizing within run variation in MBE. In this work, we present data showing the effects of rotation rate on within run variation for production pHEMT wafers. Also included is a basic model for calculating an optimal rotation rate for a given epitaxial structure.**

## INTRODUCTION

Minimizing both within-wafer and wafer-to-wafer variation is an area of continuous improvement in MBE. These variations include, but are not limited to, doping, thickness, compositions, temperature uniformity, HBT current gain and pHEMT pinch-off voltage. The geometries of MBE sources and substrates are designed to minimize variation while the substrate is rotated.[1] Continuous azimuthal rotation is necessary to improve within wafer uniformity as well as uniformity across multiple wafers for large multi-wafer production systems. Finding the optimal substrate rotation speed which minimizes variation while not over-stressing the tool can be challenging. Manipulator rotation is not always necessary in small research-oriented MBE systems but as tools grow larger, rotation effects are amplified. Manipulator rotation has been found to be very important at RFMD which runs 7x6" MBE systems for both HBT and pHEMT production.

Compositional oscillations in the growth direction and material distribution across the platen as a function of substrate rotation speed have been studied in depth.[2-4] For thick layer devices, this effect is averaged out by the large number of rotations that take place during growth. Thin layer devices grown by MBE such as AlGaAs/InGaAs QW for IR detectors, VCSELs, QCLs, spatial light modulators (SLMs) and, in the case of this work pHEMTs, need precise control of layer thickness and compositions. Here, we look at the effect of rotation speed on various pHEMT characterization and fab parameters including sheet resistance and pinch-off voltage (Vpo).

## PHEMT STRUCTURE

A typical pHEMT structure consists of the eight layers illustrated in Figure 1. The cap, Schottky and buffer layers (1, 2 & 4 in Figure 1) are thick enough so that there are a large number of rotations during the layer growth and rotation effects are averaged out at a typical rotation rate. Rotation effects are amplified during the growth of the remaining five thin layers (group 3 of Figure 1) which consist of the lower charge layer (LCL), lower spacer layer (LSL), channel, upper spacer layer (USL), and upper charge layer (UCL). Uniformity is very important during the growth of these five layers because they control the critical pHEMT pinch-off voltage.

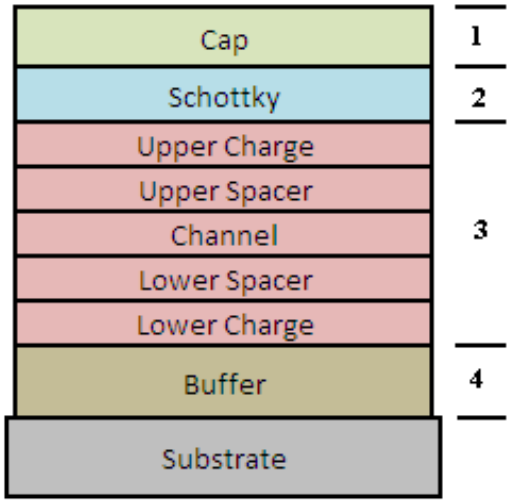


Figure 1. Schematic of a typical pHEMT structure. The five short duration layers (group 3) from the lower charge layer to the upper charge layer were the main contributors to the rotation dependent variations.

## OBSERVED ROTATION EFFECTS

The first observed rotation effect on the pHEMT structure was a wafer-to-wafer sinusoidal pattern in sheet resistance (see Figure 2) as measured using the non-contact Lehighton Model 1510ERS sheet resistance measurement and mapping system. All RFMD pHEMT wafers are tested using a 14 point-per-wafer sheet resistance scan. The sheet resistance supplies information about both layer doping and layer thickness. Historical data of RFMD's pHEMT wafers has shown that the doping of the thin charge layers has a significant impact on the average wafer sheet resistance. This same sinusoidal pattern was seen across multiple production systems with the only difference being a shift in the phase of the pattern. The average wafer-to-wafer variation was similar across multiple systems as well. This shift in phase as well as similarity of the magnitude of the variation across multiple pHEMT production systems

pointed to rotation as a possible cause. At 25 RPM, the wafer-to-wafer sheet resistance standard deviation was around 0.4%.

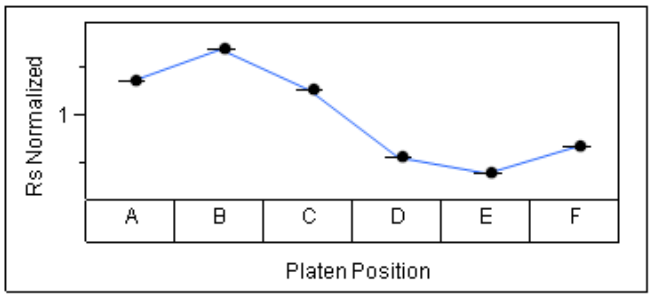


Figure 2. Sample sinusoidal variation in sheet resistance across outer wafers due to rotation effects at 25 RPM.

The simplest method to improve within-run Rs variation was to increase the rotation rate during these short duration layers from 25 RPM to 50 RPM. Doing so immediately improved the wafer-to-wafer uniformity as shown in Figure 3. The wafer-to-wafer sheet resistance standard deviation improved to 0.25% when rotated at 50 RPM. This increase in rotation rate for these short duration layers decreased the overall Rs StDev% from 0.93% to 0.76% and Cp and Cpk increased by 24% and 22% respectively.

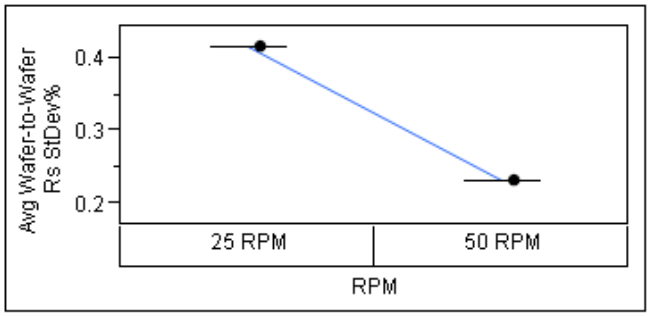


Figure 3. Over 40% improvement in wafer-to-wafer sheet resistance StDev% after doubling the rotation speed in the short duration layers to 50 RPM.

To emphasize the link between rotation rate, sheet resistance and Vpo, a run with short duration layer rotation rate of 12 RPM was grown and processed. Figure 4 shows the normalized sheet resistance and Vpo data from this run. The Vpo had the same pattern as the sheet resistance indicating that the doping variation caused by rotation not only produced a sinusoidal pattern to the sheet resistance, but also the Vpo. For this run, the wafer-to-wafer Rs StDev% was 0.6% and the wafer-to-wafer Vpo StDev% was 3.2%. When the production rotation rate was increased from 25 to 50 RPM, the Rs variation immediately improved but there was little Vpo improvement. To explain why, a rotation effects model was developed.

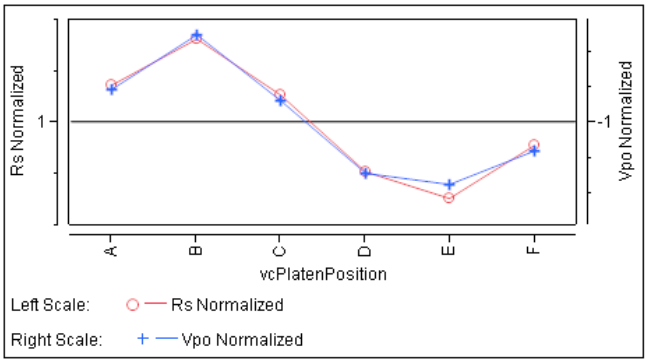


Figure 4. Normalized sheet resistance and Vpo by platen position for a pHEMT whose short duration layers were rotated at 12 RPM.

## Rotation Effects Model

To model the rotation effects, special engineering structures were grown to find the material distribution across the platen with no rotation. This was done for the Ga, Al, and Si cells. A GaAs/AlAs superlattice structure with no rotation was grown to find the Ga and Al deposition rates using x-ray mapping analysis. A superlattice structure with alternating rotating GaAs and non-rotating Si planar-doped layers was grown to find the doping profile across the platen using the Lehighton sheet resistance mapping system. The In profile was modeled to match the Al profile with growth rate corrections. Figure 5 shows the normalized Ga growth rate across the platen. As expected, the highest deposition rate on the platen occurs closest to the effusion cell location.

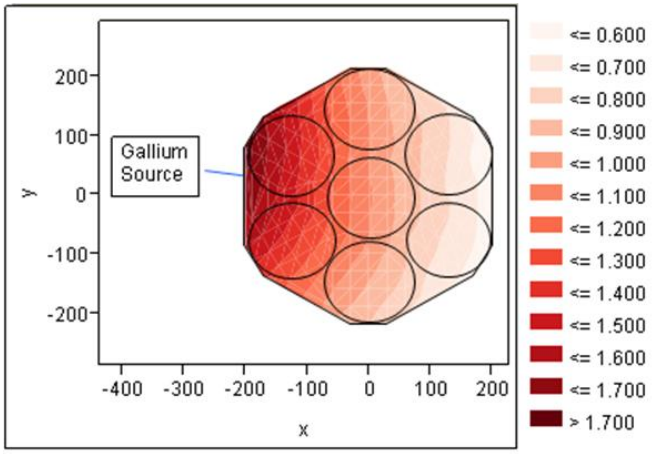


Figure 5. Normalized Ga growth rate with no substrate rotation.as measured by x-ray diffraction.

The measured deposition rate across the platen agreed well with the theoretical cosine distribution. To simplify the model, the growth rate pattern across the platen, with rotation included, was approximated with a planar distribution. Since only azimuthal effects are being studied, the planar distribution approximation is sufficient (see comparison in Figure 6). The planar distribution is given by the following equation:

$$GR_1(r,\theta,t) = \left(A_1 r \sin\left[(\theta - \theta_1) + \frac{2\pi * RPM * t}{60}\right] + 1\right) * GR_1 Offset \qquad \text{(Eq. 1)}$$

where $A_1$ is a calculated amplitude factor based on the fit of the full platen growth rate data, r is the distance from the center of the platen, θ is the azimuthal angle, $\theta_1$ is the phase shift based on the effusion port location, RPM is the platen rotation rate, t is time in seconds, and $GR_1$Offset is the deposition rate in the center of the platen as well as the average deposition rate over the whole platen. The A factor for each cell tested was close to $3x10^{-3}$/mm.

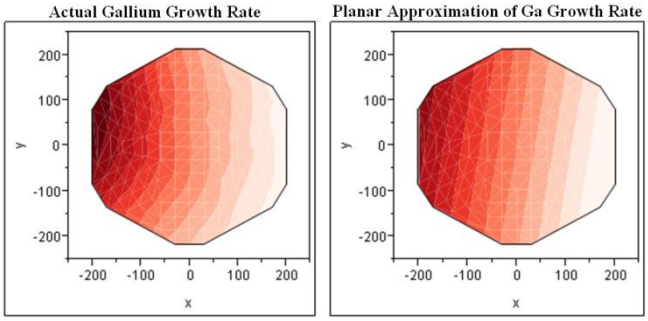


Figure 6. Comparison of measured Ga growth rate with planar Ga growth rate approximation.

The total thickness of a layer is simply found by integrating the growth rate equation with respect to time. The thickness of a layer of duration t=t1 to t2 is given by the following equation:

$$Thickness_1(r,\theta) = \int_{t1}^{t2} GR_1 dt \qquad \text{(Eq. 2)}$$

where t1 and t2 are the starting and ending times of the specific epitaxial layer in seconds. Figure 7 shows a sample map of the normalized doping of a 15.6s layer grown at 25 RPM which results in 6.5 rotations. This emphasizes the significant amount of variation across the platen at a non-integral number of rotations for a thin layer.

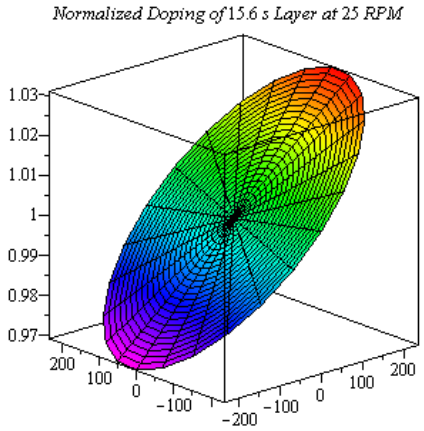


Figure 7. Sample 3D map of doping of a 15.6s layer at 25 RPM which corresponds to 6.5 rotations. This non-integral number of rotations results in doping variation of +/-3% across the platen.

By setting the value of r constant, overlays of composition, thickness and doping for various RPM values can be plotted. Figure 8 shows the normalized doping of the lower and upper charge layers at an arbitrary low RPM value.

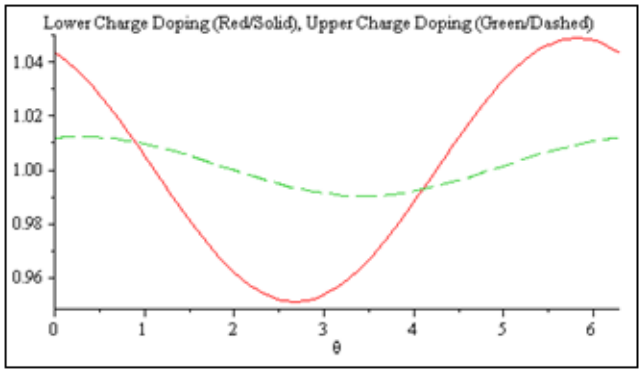


Figure 8. Sample 2D map (constant r and RPM value) which overlays the doping concentration of the lower and upper charge layers. The x-axis (θ) is the angle around the platen. With six outer wafers in a 7x6" system, each π/3 angle increment corresponds to a single wafer.

As the RPM value increases, the number of rotations for a given layer also increases, dampening the wafer-to-wafer variation. However, at an integral number of rotations the azimuthal variation drops to zero regardless of rotation rate. A qualitative representation of this effect for two different layers as a function of RPM is shown in Figure 9.

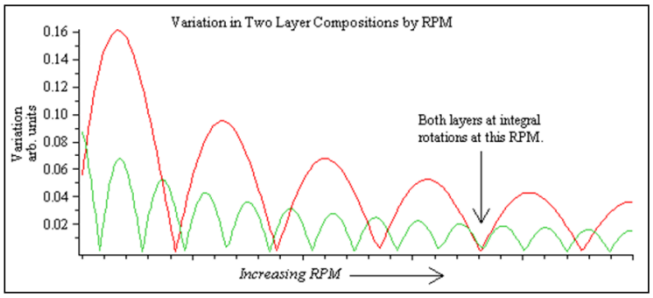


Figure 9. Overlay of compositional variation of two different layers as a function of rotation rate. Each local minimum represents a rotation rate where there are an integral number of rotations. The high amplitude/low frequency curve represents a thinner layer while the low amplitude/high frequency curve represents a thicker layer. A rotation rate where both layers are grown with an integral number of rotations (both at local minima) is noted in the plot.

With the epitaxial structure already set, it may not be possible to optimize all layers simultaneously due to limits on rotation rates.

The model showed that there was an out-of-phase relationship between the doping of the LCL and UCL at 25 RPM but an in-phase relationship at 50 RPM (see Figure 10). At 50 RPM, the doping variation of the LCL and UCL, though much smaller than the 25 RPM variation due to the extra number of rotations, were in-phase amplifying the carrier variation in the channel. This helped explain the lack

of improvement in wafer-to-wafer Vpo uniformity when the rotation rate was doubled.

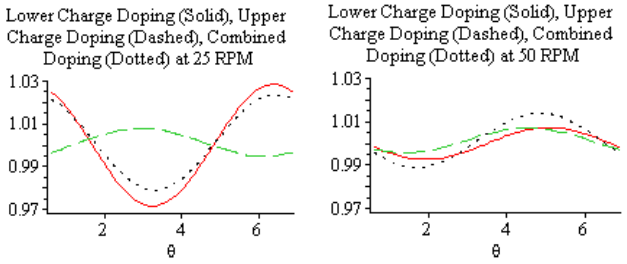


Figure 10. Comparison of normalized LCL, UCL, & combined doping at 25 & 50 RPM. The out-of-phase relationship between the LCL and UCL doping at 25 RPM had a dampening effect on the carrier contribution variation around the platen while at 50 RPM the in-phase relationship amplified the carrier concentration variation around the platen.

## Rs Improvement After Modeling

By summing the variation of each layer being studied, an optimal rotation rate can be selected. A compromise rotation rate for the RFMD pHEMT structure was found to be 46.2 RPM. This rotation rate resulted in an integral number of rotations for four of the five short duration layers. Though this rotation rate did not produce integral rotations for all five of the short duration layers of the pHEMT, it did produce the least amount of thickness and doping variation across the platen at a usable rotation rate. Upon implementing this new rotation rate, the wafer-to-wafer Rs StDev% improved further to 0.16%, an additional 36% improvement over the 50 RPM variation and a 60% improvement over the original 25 RPM variation (see Figure 11). Initial results of processed wafers also show improvement in wafer-to-wafer variation of several important pHEMT parameters including Idmax, Ron, and Vpo.

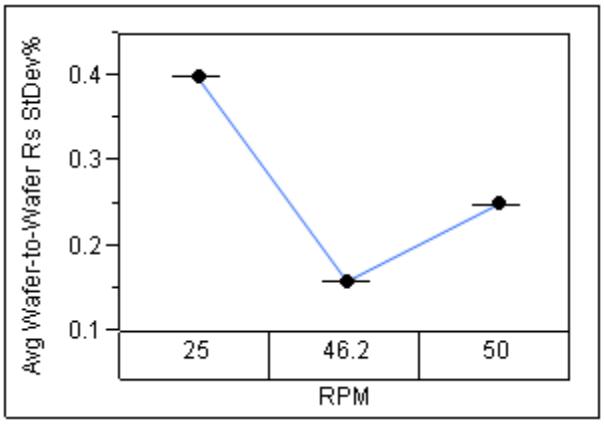


Figure 11. Comparison of wafer-to-wafer Rs StDev% for the three different rotation rates used. The compromise 46.2 RPM rotation rate for the short duration pHEMT layers resulted in Rs StDev significantly lower than the faster rotation rate of 50 RPM.

## Conclusions

We have shown that the simplest method to minimize rotation effects is in the epitaxial development stage where there is some freedom to modify the epitaxy layers in such a way that each layer is grown with an integral number of rotations. With typical MBE growth rates on the order of 3Å/s, layers that are rounded in thickness to the nearest 3Å can be grown with an integral number of rotations if the substrate rotation rate is kept at 60 RPM. It is important to note that the methods illustrated in this paper work only for a manipulator with a servomechanism motor using a motion control feedback loop. This ensures that the manipulator rotation rate and position can be predicted with confidence over extended periods of time.

If the epitaxial structure has already been developed, there are two methods for improving wafer-to-wafer uniformity that do not involve changing the epitaxial structure. The first, more crude method is to simply increase the rotation rate so that during a given layer, the wafers pass by each effusion cell more times thus increasing the number of mole fraction oscillations in the growth direction and minimizing variation. The second and more refined method is to use a model of the epitaxial structure to find a compromise rotation rate which ensures good wafer-to-wafer uniformity. For the RFMD pHEMT structure, changing the rotation rate to 46.2 RPM for the growth of the five critical short duration layers ensured the best thickness and doping uniformity. Upon implementing this new rotation rate, wafer-to-wafer as well as within-wafer variation improvement was observed due to the enhanced azimuthal uniformity.


## Acknowledgements

The authors would like to thank the RFMD MBE production group for assistance with epitaxial growth and characterization of the wafers grown as well as the RFMD wafer processing fab for their work processing the wafers. Also special thanks to MBE engineers Luke Holbert, Bob Yanka, and Wayne Lewis for their assistance.


## References


[1] A.Y. Cho and K.Y. Cheng, Appl. Phys. Lett. **38** (5), 1981.
[2] K. Alavi, P. M. Petroff, W. R. Wagner, and A. Y. Cho, J. Vac. Sci. Technol. B, **1** (2), 1983.
[3] S. N. G. Chu, N. Chand, D. L. Sivco, and A. T. Macrander, J. Appl. Phys. **65** (10), 1989.
[4] S. P. Svensson and F. J. Towner J. Vac. Sci. Technol. B, **12** (2), 1994.


## Acronyms

MBE: Molecular Beam Epitaxy
pHEMT: Pseudomorphic High Electron Mobility Transistor
HBT: Heterojunction Bipolar Transistor
QW: Quantum Well
IR: Infrared
VCSEL: Vertical Cavity Surface Emitting Laser
QCL: Quantum Cascade Laser